Conf-910414--34

To be Presented at the Advances in Mathematics, Computations, and Reactor Physics International Topical Meeting, Greentree Marriott, Pittsburgh, PA USA

ANL/CP--71385

DE91 010796

The DIF3D Nodal Kinetics Capability in Hex-Z Geometry-- Formulation and Preliminary Tests

T. A. Taiwo and H. S. Khalil

Reactor Analysis Division
Argonne National Laboratory
9700 South Cass Avenue
Argonne, IL 60439
(708) 972-7266

* Work supported by the U.S. Department of Energy, Nuclear Energy Programs under Contract W-31-109-ENG-38.

The DIF3D Nodal Kinetics Capability in Hex-Z Geometry -- Formulation and Preliminary Tests

T. A. Taiwo and H. S. Khalil
Reactor Analysis Division
Argonne National Laboratory
Argonne, Illinois 60439, U.S.A.

ABSTRACT

The development of a 3-D space- and energy-dependent neutron kinetics capability in Hexagonal-Z geometry is described. The code makes use of the nodal Hex-Z spatial differencing technique implemented in the ANL DIF3D code and, at present, the theta method for time integration. Results of numerical test problems are presented to verify the formulation of the kinetics code and to demonstrate its accuracy. The nodal differencing scheme is shown to yield more accurate transient results than does the standard (six triangle per hexagon) finite-difference scheme, which is considerably less efficient. Kinetics experiments conducted at the Savannah River Site have also been successfully analyzed using the nodal kinetics code. The time evolution and the asymptotic magnitudes of the flux tilts induced and measured in these experiments were predicted with good accuracy using the published cross section data and kinetics parameters.

INTRODUCTION

The accurate simulation of many classes of reactor transients is known to require the application of space- and energy-dependent neutron kinetics methods. Predictions obtained by point kinetics are known to be particularly unreliable for large, weakly-coupled thermal reactors when local perturbations cause pronounced changes in flux shape. In this paper, we describe the development of a spatial kinetics code for 3-D transient analysis of reactors with hexagonal unit cells and describe comparisons performed against numerical and experimental results to verify the formulation and to measure its accuracy.

The Hex-Z kinetics method described here is based on the DIF3D nodal diffusion method developed by Lawrence [1]. This method has been shown to be significantly more efficient than the conventional, finite-difference (Triangular-Z) method. The near-term application of the kinetics code is the analysis of heavy water production reactor transients, including postulated severe accidents. A parallel effort is underway [2] to develop cross section homogenization and correlation techniques needed to incorporate the DIF3D kinetics code as a computational module in the integrated HWR dynamics code SAS-HWR [3]. Future applications to liquid-metal fast reactors and gas-cooled thermal reactors are also envisioned.

MATHEMATICAL FORMULATION

Starting with the space- and time-dependent multigroup neutron balance equations, along with appropriate initial and boundary conditions, spatially discrete equations are developed in complete analogy with the static DIF3D Hex-Z nodal diffusion scheme [1]. The reactor is first partitioned into

hexagonal unit cells (lattice pitch = h) and axially subdivided into an arbitrary number of segments, resulting in a set of K nodes (right hexagonal prisms) with the height of node k denoted by Δz^k. Following reference 1, a set of time-dependent neutron balance and moment equations can be derived for each node k:

(1) The nodal balance equation:

$$\frac{1}{v_g}\frac{d}{dt}\bar{\phi}_g^k(t) + \Sigma_g^{r,k}(t)\bar{\phi}_g^k(t) = \bar{Q}_g^k(t) - \frac{2}{3h}[\bar{L}_{gx}^k(t) + \bar{L}_{gu}^k(t) + \bar{L}_{gv}^k(t)] - \frac{1}{\Delta z^k}\bar{L}_{gz}^k(t) \ . \tag{1}$$

(2) The moment equation for hex-plane coordinate direction x:

$$\frac{1}{v_g}\frac{d}{dt}\phi_{g,x1}^k(t) + [\Sigma_g^{r,k}(t) + \frac{32}{h}\frac{D_g^k(t)}{h}]\phi_{g,x1}^k(t) = Q_{g,x1}^k(t) - \frac{1}{\Delta z^k}L_{gz,x1}^k(t)$$

$$- \frac{2}{3h}[\bar{T}_{gx}^k(t) + \bar{T}_{gu}^k(t) - \bar{T}_{gv}^k(t)] + \frac{40}{9h}\frac{D_g^k(t)}{h}[\bar{\phi}_{gx}^k(+\frac{h}{2},t) - \bar{\phi}_{gx}^k(-\frac{h}{2},t)] \ . \tag{2}$$

(Corresponding equations can be written for hex-plane directions u and v, which are rotated 60 and 120 degrees, respectively, from the x direction)

(3) The moment equation in the axial (z) direction:

$$\frac{1}{v_g}\frac{d}{dt}\phi_{g,z1}^k(t) + \Sigma_g^{r,k}(t)\phi_{g,z1}^k(t) = [Q_{g,z1}^k(t) - \frac{2}{3h}L_{gxy,z1}^k(t)] - \frac{1}{2\Delta z^k}\bar{T}_{gz}^k(t)$$

$$- \frac{D_g^k(t)}{\Delta z^k}\frac{1}{\Delta z^k}[\bar{\phi}_{gz}^k(+\frac{\Delta z^k}{2},t) - \bar{\phi}_{gz}^k(-\frac{\Delta z^k}{2},t)] \ . \tag{3}$$

In these equations, for each group g and node k, Q_g^k denotes the neutron source from fission (prompt plus delayed source) and in-scatter, L_{gs}^k is the net leakage in coordinate direction s (difference between the s-directed, surface-averaged net currents at the two opposite surfaces perpendicular to direction s), T_{gs}^k is the corresponding sum of the s-directed net currents at opposite node surfaces, L_{gxy}^k is the z-dependent net leakage transverse to the z direction (i.e. in the hex-plane), and $\bar{\phi}_{gs}^k$ is the flux averaged over the specified surface perpendicular to direction s. The bar above a variable denotes its average value, while the subscript "s1" denotes the spatial moment of a variable, taken along coordinate direction s (s = x, u, v, or z). The remaining notation is standard. It should be noted that in the numerical solution of these equations, the surface-averaged fluxes and net currents are eliminated in favor of incoming and outgoing surface-averaged partial currents, $J_{gs}^{out,k}$ and $J_{gs}^{in,k}$, respectively.

A corresponding set of balance and moment equations can be derived for the delayed neutron precursors belonging to precursor family d in node k. Assuming that the production cross section, the delayed neutron fraction β_d, and the decay constant λ_d for each delay group d have been appropriately averaged (i.e. are constant within a node) and neglecting the possibility of delayed neutron precursor migration, the precursor balance and moment equations can be written in vector form as:

$$\frac{d}{dt}\underline{C}_d^k(t) = \sum_{g'=1}^{G}\beta_d^k\frac{\nu}{\gamma}\Sigma_{g'}^{f,k}(t)\underline{\phi}_{g'}^k(t) - \lambda_d\underline{C}_d^k(t) \qquad d=1,2,\ \ldots\ ,D\ , \tag{4}$$

where $\underline{C}_d = col\{\overline{C}_d, C_{d,x1}, C_{d,u1}, C_{d,v1}, C_{d,z1}\}$, C_d being the concentration of precursors belonging to delay group d, and where $\underline{\phi}_g = col\{\overline{\phi}_g, \phi_{g,x1}, \phi_{g,u1}, \phi_{g,v1}, \phi_{g,z1}\}$.

In reference 1, the time-independent forms of Eqs. (1), (2), and (3) are solved along with "response matrix" equations derived by first representing 1-D (transverse-averaged) fluxes in the hex-plane directions (u, v, and w) and in the z-direction using up to four polynomial basis functions. The coefficients of these functions are eliminated by requiring the flux expansion to (1) preserve the node-averaged and node surface-averaged fluxes, (2) yield net current continuity at the surfaces formed by the intersection of the node with the vertical planes x=0, u=0, and v=0, (3) satisfy nodal balance over each of the two pairs of half nodes formed by each of these vertical surfaces, and (4) preserve the first z-moment of the 1-D, z-dependent flux. In addition, the planar leakage (transverse to the z-direction) is approximated by a quadratic polynomial, while the leakage transverse to each hex-plane direction is treated by a "two-step" approximation [1]. Finally, surface fluxes and net currents are eliminated in favor of surface incoming and outgoing partial currents to obtain the desired response matrix equations.

By adopting the same set of approximations in the present (time-dependent) application, we can write the resulting response matrix equations in the form

$$\underline{J}_g^{out,k}(t) = [X_g^k(t)]\underline{\phi}_g^k(t) + [Y_g^k(t)]\underline{J}_g^{in,k}(t)\ , \tag{5}$$

where the elements of the coupling coefficient matrices $[X_g^k(t)]$ and $[Y_g^k(t)]$ are defined by the dimensions and time-dependent cross sections of node k, and where $\underline{J}_g^{out,k}$ and $\underline{J}_g^{in,k}$ are column vectors containing the surface-averaged outgoing and incoming partial currents, respectively, for all eight node surfaces. Note that Eq. (5) is an instantaneous relation between the partial currents and flux moments with time appearing only as a parameter. This relation is analogous to the flux-current relation implicit in time-dependent diffusion schemes, in which the time derivative of the net current (appearing in the time-dependent P-1 equations) is neglected.

Time discretization of the flux moment equations, Eqs. (1) to (3), was accomplished by applying the θ – method [4,5] which permits the resulting difference equations to range from fully explicit when $\theta = 0$ to fully implicit when $\theta = 1$; the Crank-Nicholson scheme is obtained when $\theta = 1/2$. For example, application of the θ – method to the nodal balance equation, Eq. (1), yields

$$\begin{aligned}\frac{1}{v_g\Delta t_n}(\overline{\phi}_g^{k,n+1} - \overline{\phi}_g^{k,n}) + \theta\Sigma_g^{r,k,n+1}\overline{\phi}_g^{k,n+1} + (1-\theta)\Sigma_g^{r,k,n}\overline{\phi}_g^{k,n} \\ = \theta\overline{Q}_g^{k,n+1} + (1-\theta)\overline{Q}_g^{k,n} - \frac{2\theta}{3h}[\overline{L}_{gx}^{k,n+1} + \overline{L}_{gu}^{k,n+1} + \overline{L}_{gv}^{k,n+1}] \\ - \frac{2(1-\theta)}{3h}[\overline{L}_{gx}^{k,n} + \overline{L}_{gu}^{k,n} + \overline{L}_{gv}^{k,n}] - \frac{\theta}{\Delta z^k}\overline{L}_{gz}^{k,n+1} - \frac{(1-\theta)}{\Delta z^k}\overline{L}_{gz}^{k,n}\ ,\end{aligned} \tag{6}$$

where $\Delta t_n = t_{n+1} - t_n$, and the superscript n denotes quantities evaluated at t_n .

The delayed neutron precursor equations can be integrated directly assuming that the production of precursors by fission is a linear function of time within each time step. The resulting equation

is

$$\underline{C}_d^{k,n+1} = \underline{C}_d^{k,n} e^{-\lambda_d \Delta t_n} + \sum_{g'=1}^{G} \frac{\beta_d^{k,n+1}}{\lambda_d} \frac{\nu}{\gamma} \Sigma_{g'}^{f,k,n+1} \underline{\phi}_{g'}^{k,n+1} \left\{ 1 - \frac{1}{\lambda_d \Delta t_n} (1 - e^{-\lambda_d \Delta t_n}) \right\}$$

$$+ \sum_{g'=1}^{G} \frac{\beta_d^{k,n}}{\lambda_d} \frac{\nu}{\gamma} \Sigma_{g'}^{f,k,n} \underline{\phi}_{g'}^{k,n} \left\{ \frac{1}{\lambda_d \Delta t_n} (1 - e^{-\lambda_d \Delta t_n}) - e^{-\lambda_d \Delta t_n} \right\} . \qquad (7)$$

Using Eqs. (6) and (7) (and equations analogous to (6) for the flux moments), expressions can be obtained for the flux moments at time t_{n+1} in terms of the partial currents, and the fission and scattering source moments at time t_{n+1} , as well as a "fixed" source term that is composed using information from the preceding time (t_n) solution. These expressions can be used to eliminate the flux moments appearing in the response matrix equation in favor of the partial currents and source terms. The resulting set of response matrix equations is then of the form

$$\underline{J}_g^{out,k,n+1} = [P_g^{k,n+1}] \{ \underline{Q}_g^{k*,n+1} - \underline{L}_g^{k,n+1} \} + [R_g^{k,n+1}] \underline{J}_g^{in,k,n+1} . \qquad (8)$$

Although Eq. (8) is of the same form as the expression derived by Lawrence in reference 1, the coefficient matrices $[P_g^{k,n+1}]$ and $[R_g^{k,n+1}]$ are different; for example, the coefficients here depend on the the quantities θ and Δt_n and on the kinetics parameters. Furthermore, the vector $\underline{Q}_g^{k*,n+1}$ contains the fission and scattering source terms for the present time t_{n+1} ,as well as another component that contains the previous time information. Equation (8) can be solved together with Eq. (6) and its moment counterparts to advance the flux solution from t_n to t_{n+1} .

To initiate the solution, an eigenvalue problem is solved at $t = 0$, subject to specified boundary conditions, using the time-independent algorithm of DIF3D nodal [1]. The resulting initial flux distribution is normalized to the specified input power level. At each subsequent time point, the response matrix equation and the flux moment expressions are solved iteratively with the aid of the fixed source algorithm of the DIF3D nodal code [6]. The fixed source at each time point depends entirely on the previous time point information. The unknown flux moments and interface partial currents are computed using a conventional fission source iteration accelerated by coarse-mesh rebalance and asymptotic source extrapolation. At each fission source iteration, the interface partial currents for each group are computed by solving the response matrix equations with a known group source term. Special coding was needed to accomodate the fully explicit scheme, for which the coupling coefficients had to be calculated differently (to avoid division by zero), and only the response matrix iteration (no fission source iteration) is required at each time point. Numerical test cases done to date show that the iteration strategy in the DIF3D nodal code is very effective for time-dependent problems; no problem has failed to converge due to the iterative scheme.

A transient solution acceleration technique was implemented, in which the flux and partial current values at the end of a given time are extrapolated exponentially to give an initial guess of the unknowns at the next time point. An automatic time-stepping option was also included in the code. This option constrains the maximum time step size Δt so that the product of Δt and the instantaneous inverse period in all nodes is less than a user-specified value.

Because the DIF3D-nodal kinetics capability has been designed to be a computational module in an integrated dynamics code (such as SAS-HWR), no reactor-specific thermal-hydraulic or cross section feedback models have been included within the code. Instead, the code makes use of macroscopic cross sections and kinetics parameters specified at each time point during a transient.

NUMERICAL VERIFICATION

Because of the lack of published benchmark-quality solutions of kinetics problems in 3-D Hex-Z geometry, verification tests have so far been restricted to demonstrating that the 3-D Hex-Z nodal kinetics code correctly and efficiently solves problems of lower spatial dimensions (e.g. 1-D axial problems and 2-D hexagonal geometry problems), as well as problems where the (3-D) space and time dependencies are separable. Furthermore, some 3-D test cases have been run and the solutions compared to published results to confirm the ability of the code to analyze transient problems in Hex-Z geometry. Some results of the various test cases are presented in this section.

1-D Delayed Super-Critical Transient

A one-dimensional delayed super-critical transient benchmark problem [7] simulating a loosely-coupled reactor has been used to test the accuracy and capabilities of the code. In this problem, the initial flux distribution is peaked at the edges and severely depressed at the center. The transient resulted from locally decreasing the absorption cross section in one edge region of the reactor over one second, resulting in a pronouced flux shape change. The problem was modelled as a 3-D, two-ring, axially heterogenous problem with zero net current boundary in the hex-plane, and zero flux boundary in the Z-direction. As shown in Table 1, the nodal solution with a coarse axial node size of 20 cm (12 axial nodes) agrees closely with the reference fine-mesh results. The achievement of comparable accuracy with a finite-difference code requires a mesh size of approximately 1.0 cm and substantially more computing effort. Note from Table 1 that the flux extrapolation technique and the automatic time-stepping options reduce computation time significantly.

2-D Test Cases

A consistent comparison between the DIF3D-nodal kinetics code and the 2-D finite-difference (quasi-static) kinetics code FX2-TH [8] was performed using the 2-D reactor configuration shown in Figure 1. This configuration is very similar to the HWR experiment configuration described in reference 9. Cross section data and kinetics parameters for this problem were taken from reference 9 and are given in Table 2. The loading of the reactor is such that the flux is peaked in the outer control gang (gang 3) near the core periphery.

Two different transient test cases were analyzed. The first case provides a difficult test for a spatial kinetics code. This test simulates the dropping of two fuel bearing rods (per 60-degree sector) into control gang 3, where the flux is peaked, producing a local perturbation in a high-leakage core location; the duration of the drop is 0.205 s. A reference solution was obtained using a 54 triangles/hexagon (54 tri/hex) FX2-TH representation. Two additional FX2-TH calculations were performed using 6 and 24 tri/hex. Results from these calculations for the time variation of the core power level are compared with the corresponding nodal kinetics results in Figure 2. From these results, it is evident that the nodal solution is nearly as accurate as the 24 tri/hex FX2-TH solution and is considerably more accurate than the 6 tri/hex solution. Since the nodal solution requires, per time step, a factor of five to ten less computing time than the 6 tri/hex solution (and substantially less computer memory), the greater accuracy is achieved at a significantly lower computational cost.

Although the nodal scheme is significantly more cost-effective than the finite-difference approach, Figure 2 reveals that the nodal solution overpredicts somewhat the power rise as a function of time relative to the reference solution. This overprediction is a consequence of the overestimation (by 2 cents) of the reactivity (reference value = 75.5 cents). As shown in Table 3, the node-averaged total fluxes are very well predicted by the nodal solution for both the unperturbed and (asymptotic) perturbed states. However, the errors in the individual group fluxes at the perturbation

site (a local heterogeneity,) are somewhat larger as shown in Table 3 and appear to be the cause of the reactivity overprediction.

The second 2-D test case consisted of a more uniform perturbation induced by reducing the thermal absorption cross section by 4.5% (in 0.2 s) in the entire central control zone of the core. The reactivity worth of this perturbation (74.4 cents), calculated by a reference 54 tri/hex FX2-TH solution is closely matched by the DIF3D-nodal value of 74.7 cents. A comparison of the DIF3D-nodal and FX2-TH finite-difference results for the core power variation is displayed in Figure 3. Note that the nodal solution is in excellent agreement with the reference result and is again noticeably more accurate than the 6 tri/hex FX2-TH solution.

A meaningful comparison of the computing times required by DIF3D-nodal and FX2-TH for analyzing these transients cannot be made at the present time. The DIF3D kinetics code has been implemented on the ANL Cray X-MP computer, while FX2-TH is only operational on IBM computers (and is limited to 2-D applications). In addition, the DIF3D and FX2-TH code utilize different approches for treatment of the time-dependence (θ–method and quasi-static, respectively), the effectiveness of which is known to be problem-dependent and sensitive to the choice of input parameters. A quasi-static solution option is currently being implemented in DIF3D and may facilitate the inter-comparison of the two codes. Nevertheless, it seems clear that the efficiency advantage of the DIF3D nodal approach (for each flux shape recalculation) can be exploited to reduce the computational expense of performing accurate transient calculations in Hex-Z geometry.

3-D Delayed-Prompt Critical Transient

A 3-D Hex-Z kinetics test case, designated as test case III in reference 9, has also been analyzed using DIF3D-nodal; results were compared to the published results [9] calculated by the TRIMHX code using a coarse-mesh (1 cell/hexagon) finite-difference scheme. In this test problem, the thermal absorption cross section in the central core patch was reduced by 15%, producing a substantial flux rise (a factor of 135 in 5 s) in the central part of the core. In reference 9, this perturbation was calculated to produce a (static) reactivity change of 87 cents. Since the static reactivity computed by DIF3D-nodal using the specified perturbation was only 84 cents (the DIF3D value is likely to be more accurate), the DIF3D-nodal analysis of the transient was performed both for the specified 15% reduction in Σ_{a2} (i.e. DIF3D reactivity = 84 cents) and for a 15.37% reduction (matching the 87 cent reactivity insertion of reference 9). In addition, the group-2 neutron velocity was taken to be 1775 m/s in order to match the published value of the prompt neutron lifetime. Results of the two DIF3D-nodal calculations are compared with the published results in Figure 4. The DIF3D solution with the perturbation adjusted to reproduce the published reactivity worth is seen to be in excellent agreement with the published result. Figure 5 illustrates the time evolution of the thermal flux radial distribution at the reactor axial midplane as calculated by DIF3D nodal with the adjusted perturbation. This result is very similar to that presented in Figure 5 of reference 9.

COMPARISON TO EXPERIMENTAL MEASUREMENTS

Two kinetics experiments conducted in the heavy-water moderated Process Development Pile at the Savannah River Site [10] have been analyzed. These experiments measured the initial flux distribution with the aid of bare and cadmium covered gold pins, and the time-dependent flux tilts that resulted between symmetrical locations of the core with Boron-10 lined detectors. Transients were intitiated by dropping two or more U-235 bearing rods into the lattice at designated perturbation sites [10]. In the analysis, the published set [10] of two-group cell and supercell averaged macroscopic cross sections (and kinetics parameters) were used. These cross sections were calculated by the RAHAB code and used in previous TRIMHX analyses of the experiments [10].

The initial flux distributions as measured by the local gold pin activation rates were generally well predicted by DIF3D-nodal using the RAHAB cross sections. The average deviation between the measured and calculated thermal fluxes was 2.5% in Experiment 1 and 3.6% in Experiment 2. The maximum deviation of 9% in one of the gold pin locations in Experiment 2 appears to be anomalously high. The time-dependent flux tilts were well predicted except for one of the tilts in Experiment 1 in which the difference between calculated and measured asymptotic values was 5%. The agreement should be considered good because of (a) possible inaccuracies in the cross sections, (b) the use of a simple interpolation technique to determine local flux values at the detector locations from the nodal information, and (c) potential inaccuracies in measured activation rates (no uncertainties were quoted in reference 10). In addition, the nodal flux shapes calculated for the initial and final states were found to be in excellent agreement with fine mesh solutions calculated by the finite difference option of DIF3D [11].

Figure 6 shows the measured and calculated flux tilts for Experiment 2 as a function of time. The results indicate that (a) spatial kinetics code accurately models the evolution of the flux tilts (as held back by delayed neutrons), and (b) the time-dependent solution properly approaches the asymptotic tilts predicted by the static calculation for the final (perturbed) state.

SUMMARY AND PLANNED EXTENSIONS

In summary, a kinetics capability taking advantage of the efficiency of the DIF3D Hex-Z nodal method has been developed and shown to yield accurate results for numerical and experimental test cases. Work has been initiated on the development of a quasi-static code option as a means of increasing flexibility and reducing running time for transients in which the flux shape is slowly varying. In addition, the formulation is being extended to model delayed neutron precursor migration upon fuel relocation in postulated severe accident sequences.

ACKNOWLEDGEMENT

The authors are grateful to K. Derstine for providing consultation and assistance with the DIF3D code modifications.

REFERENCES

1. R. D. Lawrence, "The DIF3D Nodal Neutronics Option for Two- and Three-Dimensional Diffusion Theory Calculations in Hexagonal Geometry," ANL-83-1, Argonne National Laboratory, March 1983.

2. W. S. Yang, ANL, Private Communication, September 1990.

3. E. E. Morris, ANL, Private Communication, February 1990.

4. K. S. Smith, "An Analytic Nodal Method for Solving the Two-Group, Multidimensional, Static and Transient Neutron Diffusion Equations," M.S. and N.E. Thesis, M.I.T., March 1979.

5. A. V. Vota, N. J. Curlee, Jr., and A. F. Henry, "WIGL3 - A Program for the Steady-State and Transient Solution of the One-Dimensional, Two-Group, Space Time Diffusion Equations Accounting for Temperature, Xenon, and Control Feedback," WAPD-TM-788, February 1969.

6. K. L. Derstine, ANL, Private Communication, April 1990.

7. National Energy Software Center: Benchmark Problem Book, ANL-7416-Supplement 3, December 1985.

8. R. A. Shober, T. A. Daly, and D. R. Ferguson, "FX2-TH: A Two-Dimensional Nuclear Reactor Kinetics Code With Thermal-Hydraulic Feedback," ANL-78-97, Argonne National Laboratory, October 1978.

9. M. R. Buckner and J. W. Stewart, "Multidimensional Space-Time Nuclear-Reactor Kinetics Studies-Part I: Theoretical," NSE, 59, p. 289, 1976.

10. P. B. Parks et al, "Multidimensional Space-Time Nuclear-Reactor Kinetics Studies-Part II: Experimental," NSE, 59, p. 298, 1976.

11. K. L. Derstine, "DIF3D: A Code to Solve One-, Two-, and Three-Dimensional Finite-Difference Diffusion Theory Problems," ANL-82-64, Argonne National Laboratory, April 1984.

Table 1. Comparison of Calculated Powers for the 1-D Delayed Supercritical Transient

		Total Reactor power						
Time(s)	Ref.	Case 1	Case 2	Case 3	Case 4	Case 5	Case 6	Case 7
0.0	1.000	1.000	1.000	1.000	1.000	1.000	1.000	1.000
0.1	1.028	1.029	1.029	1.028	1.028	1.028	1.027	1.028
0.2	1.063	1.063	1.063	1.062	1.062	1.062	1.063	1.062
0.5	1.205	1.205	1.205	1.203	1.203	1.202	1.202	1.204
1.0	1.740	1.740	1.740	1.730	1.728	1.727	1.729	1.733
1.5	1.959	1.956	1.956	1.942	1.941	1.945	1.944	1.945
2.0	2.166	2.162	2.162	2.141	2.141	2.142	2.141	2.146
3.0	2.606	2.599	2.599	2.568	2.567	2.566	2.567	2.573
4.0	3.108	3.098	3.098	3.052	3.050	3.053	3.051	3.061
Axial nodes	120	48	48	12	12	12	12	12
Fission Source Convergence	NA	.00001	.00001	.00001	.00001	.001	.00001	.00001
Time step size (s)	0.001	0.100	0.100	0.100	0.010	0.100	0.100	0.100
Theta	NA	1.000	1.000	1.000	1.000	1.000	0.500	1.000
Flux Extrapolation	NA	YES	NO	YES	YES	YES	YES	YES
Automatic Time Stepping	NA	NO	NO	NO	NO	NO	NO	YES
Region		Regional Power Fractions at 4.0 seconds						
1	0.443	0.441	0.441	0.440	0.440	0.440	0.439	0.440
2	0.430	0.432	0.432	0.432	0.432	0.432	0.432	0.432
3	0.127	0.127	0.127	0.128	0.128	0.128	0.128	0.128
cpu ratio	NA	1.000	1.750	0.322	1.526	0.117	0.408	0.187

Notes:

(1) The cpu ratio is the total cpu time for case divided by total cpu time for case 1.
(2) The Reference power fraction was deduced from data in Ref. 7.
(3) All cases were run on the CRAY XMP/14 computer at ANL.

Table 2. Cross Section and Kinetics Data for the 2-D Test Cases

Composition Cross Section Data (cm^{-1})

Composition	Group	Σ_r	Σ_c	Σ_f	$\nu\Sigma_f$	$\Sigma_{1\to2}$
1	1	2.41109E-01	1.63052E-03	9.30113E-04	2.26216E-03	8.16457E-03
	2	3.71393E-01	1.25413E-02	9.51810E-03	2.30623E-02	-
2	1	2.41100E-01	1.65429E-03	9.15899E-04	2.22750E-03	8.22378E-03
	2	3.71406E-01	1.27782E-02	9.36233E-03	2.26849E-02	-
3	1	2.42527E-01	1.27299E-03	8.80841E-04	2.14281E-03	8.08816E-03
	2	3.75220E-01	8.24602E-03	8.45594E-03	2.04887E-02	-
4*	1	2.54069E-01	1.52655E-05	-	-	1.23115E-02
	2	3.78825E-01	2.86769E-04	-	-	-
5**	1	2.51572E-01	1.19371E-04	1.49854E-04	3.64898E-04	1.03583E-02
	2	3.85126E-01	8.64087E-04	2.57614E-03	6.24196E-03	-
6	1	2.41303E-01	1.43233E-03	9.84814E-04	2.39469E-03	7.76568E-03
	2	3.68866E-01	1.06673E-02	1.09869E-02	2.66211E-02	-
7	1	2.55234E-01	2.74282E-04	-	-	1.10975E-02
	2	3.98126E-01	4.10254E-03	-	-	-
8	1	2.58012E-01	1.44797E-06	-	-	1.15582E-02
	2	4.06831E-01	7.50003E-05	-	-	-
9	1	3.12960E-01	1.85500E-03	-	-	2.61980E-02
	2	1.03254E-00	3.32600E-02	-	-	-

* Site Of Dropped Rod Before the Drop. (Test Case 1 Only)
** Site of Dropped Rod After the Drop. (Test Case 1 Only)

Delayed Neutron Data

Family Number	Delayed Neutron Fraction	Decay Constant (s^{-1})
1	1.68000E-04	3.87100E-00
2	8.25700E-04	1.40000E-00
3	3.09920E-03	3.05800E-01
4	1.21090E-03	1.15000E-01
5	1.76570E-03	2.78100E-02
6	1.10900E-04	2.59800E-03

Additional data

Lattice Pitch = 17.78 cm
Buckling = 2.753E-04 cm^{-2}

	Group 1	Group 2
Prompt and Delayed Fission Spectrum	1.00000E-00	0.00000E-00
Neutron Velocity (cm/s)	1.12860E+07	3.08060E+05

Table 3. Normalized Fluxes for Test Case 1

(a) Total Flux Distribution

Hexagon Number *	Initial State (t = 0.0 sec.) DIF3D Nodal	FX2-TH 6 tri/hex	FX2-TH 54 tri/hex	Asymptotic State (t = 3.0 sec.) DIF3D Nodal	FX2-TH 6 tri/hex	FX2-TH 54 tri/hex
1	1.0000	1.0000	1.0000	1.0000	1.0000	1.0000
2	1.0144	1.0145	1.0145	1.0172	1.0174	1.0172
3	1.0583	1.0584	1.0586	1.0697	1.0703	1.0697
4	1.1337	1.1339	1.1342	1.1606	1.1620	1.1604
5	1.2437	1.2441	1.2447	1.2952	1.2979	1.2949
6	1.3932	1.3937	1.3949	1.4826	1.4872	1.4820
7	1.5924	1.5924	1.5955	1.7417	1.7482	1.7408
8	1.8881	1.8885	1.8937	2.1367	2.1480	2.1357
9	2.3414	2.3369	2.3481	2.7466	2.7606	2.7421
10	2.7883	2.7973	2.7961	3.3175	3.3547	3.3117
11	2.6672	2.6744	2.6773	3.1967	3.2328	3.1938
12	2.0027	2.0031	2.0108	2.4113	2.4335	2.4093
13	1.0856	1.0881	1.0872	1.2998	1.2971	1.2958
14	0.3966	0.3925	0.3936	0.4730	0.4721	0.4674

* Hexagon numbers increase in moving radially outward along x-axis (See Fig. 1)

(b) Group Fluxes at Perturbation Site **

	Initial State (t = 0.0 sec.) DIF3D Nodal	FX2-TH 6 tri/hex	FX2-TH 54 tri/hex	Asymptotic State (t = 3.0 sec.) DIF3D Nodal	FX2-TH 6 tri/hex	FX2-TH 54 tri/hex
Group 1	1.6603	1.6106	1.7027	2.3361	2.3311	2.3582
Group 2	4.6991	4.8686	4.5813	4.9966	5.2091	4.8804
Total	2.4789	2.4883	2.4782	3.0535	3.1071	3.0383

** Perturbation site shown in Fig.1.

Figure 1. Sixty-Degree Core Sector for the 2-D Test Cases

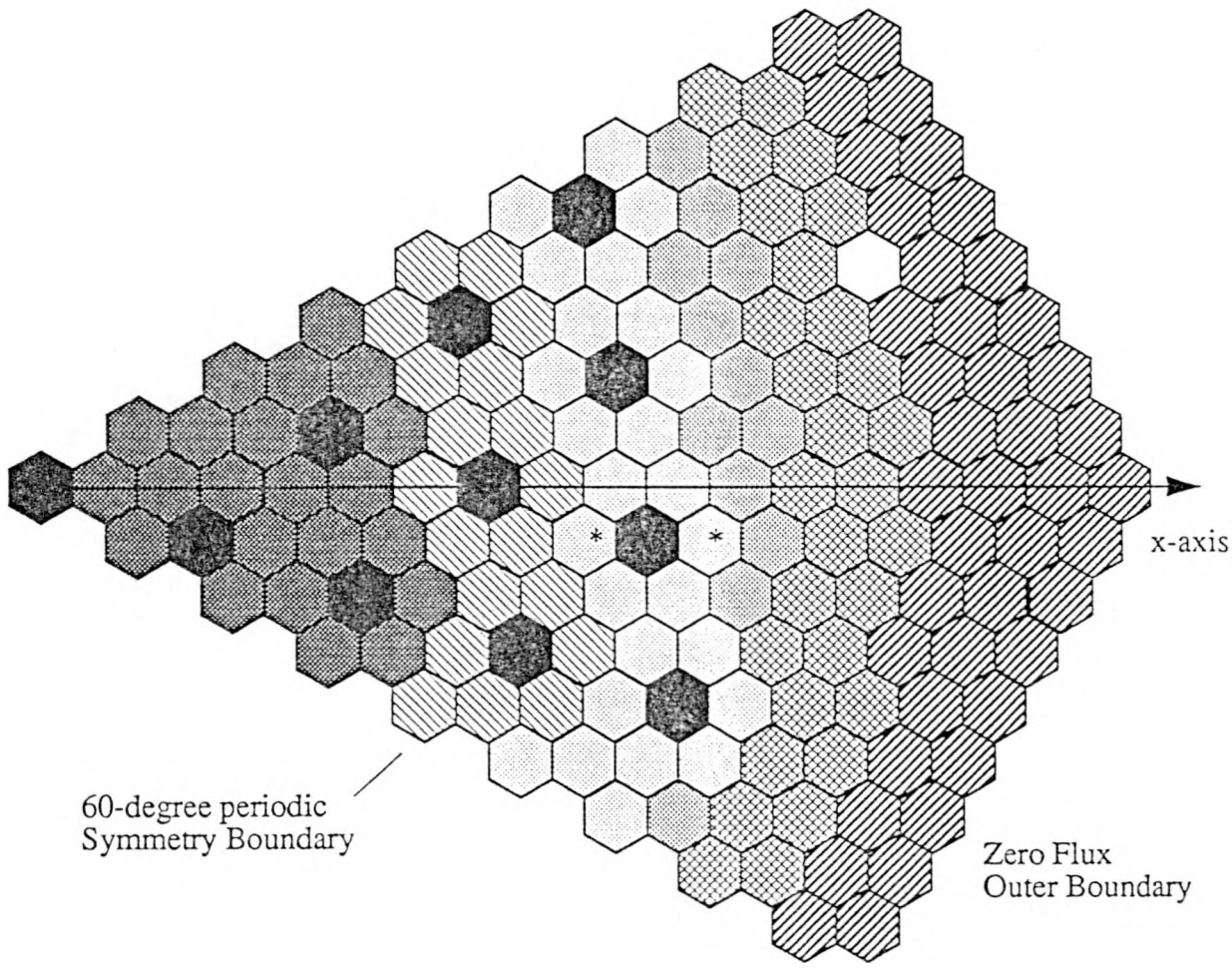

Fuel Assembly in Gang 1
(Composition 1)

Fuel Assembly in Gang 2
(Composition 2)

Fuel Assembly in Gang 3
(Composition 3)

Control Asembly
(Included in Composition 1,2 or 3)

Dropped Rod Site in Test Case 1
(Compositions 4 and 5)

Fuel in Buckled Zone
(Composition 6)

Lithium Target
(Composition 7)

Vacancy
(Composition 8)

Core Exterior
(Composition 9)

Figure 2. Core Power vs. Time for 2-D Test Case 1.

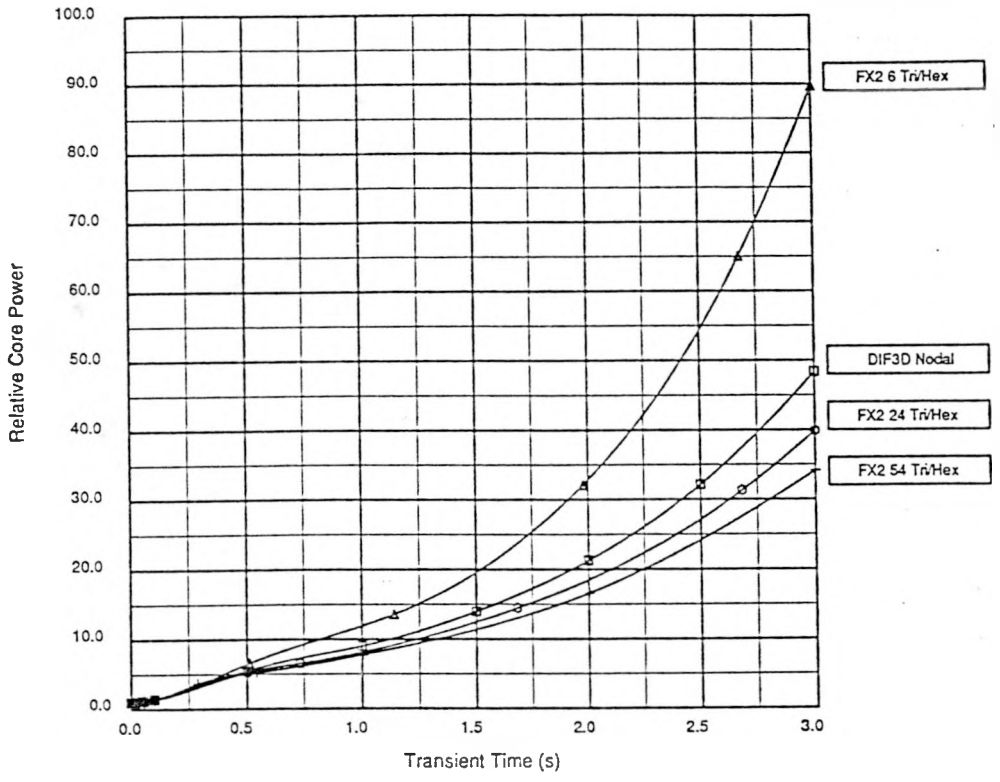

Figure 3. Core Power vs. Time for 2-D Test Case 2.

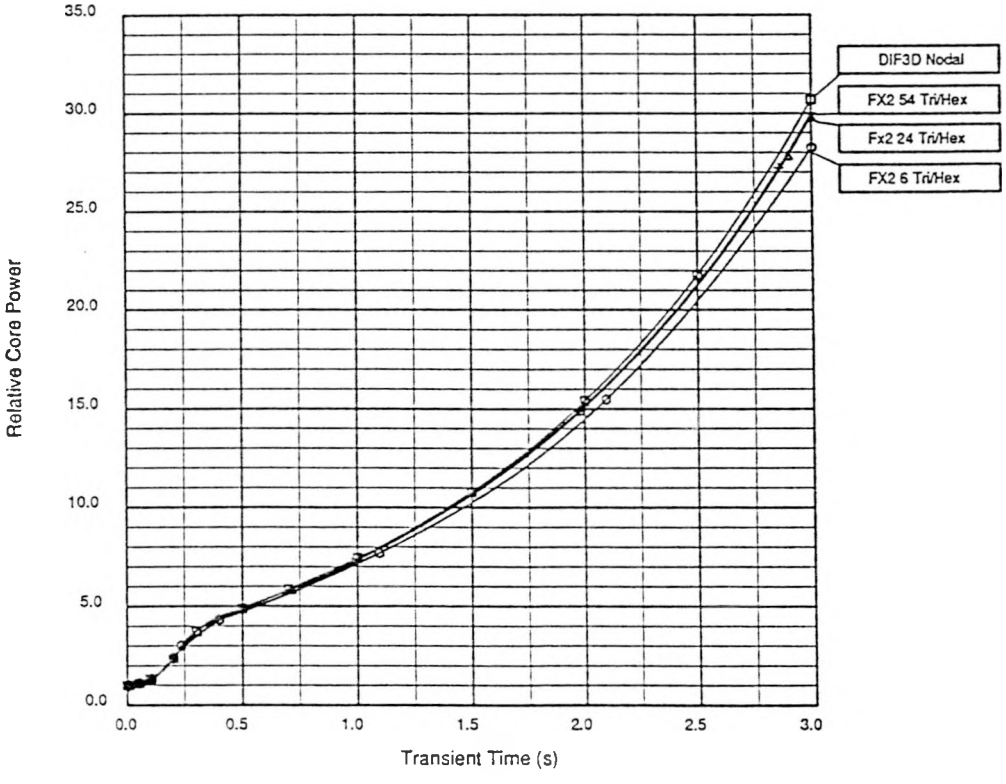

Figure 4. Relative Thermal Flux at Central Assembly Midplane vs. Time.

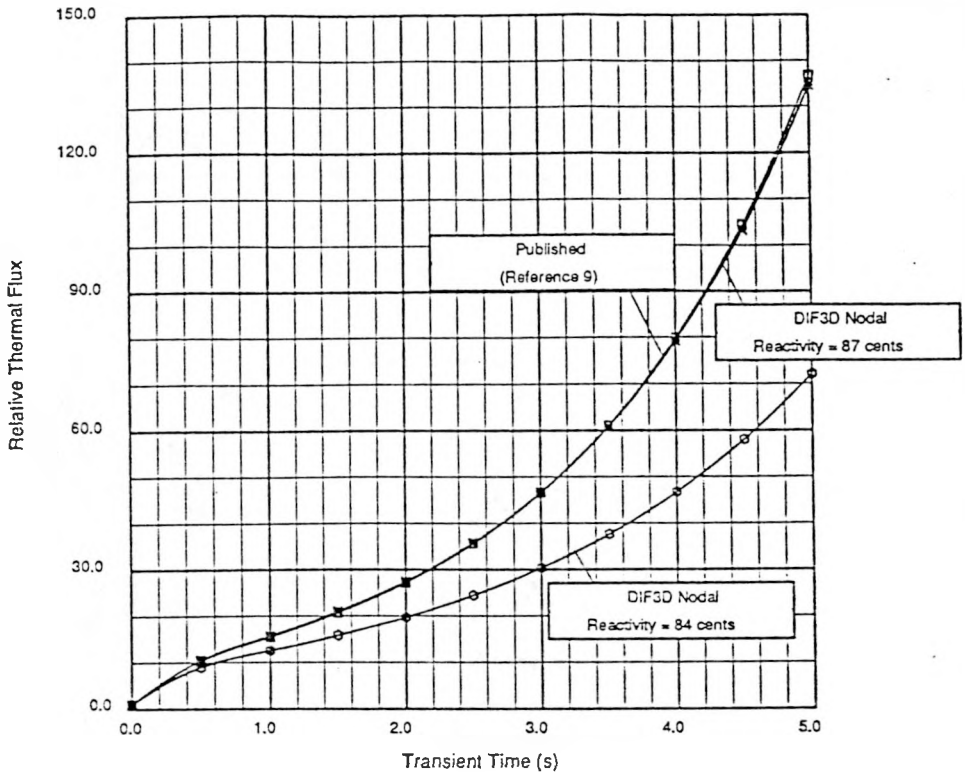

Figure 5. Thermal Flux Radial Shape at Reactor Midplane.

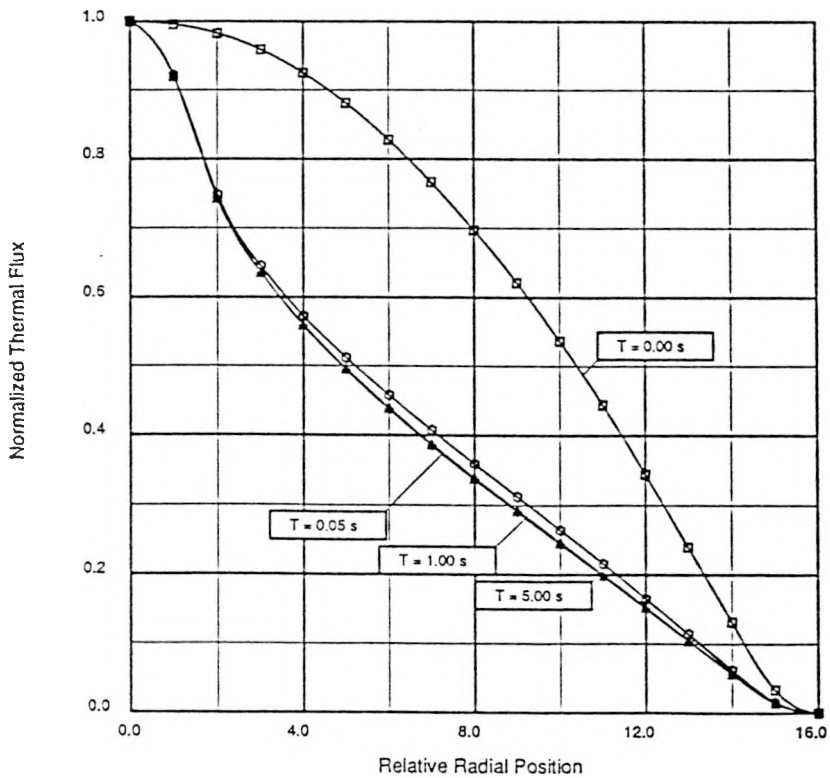

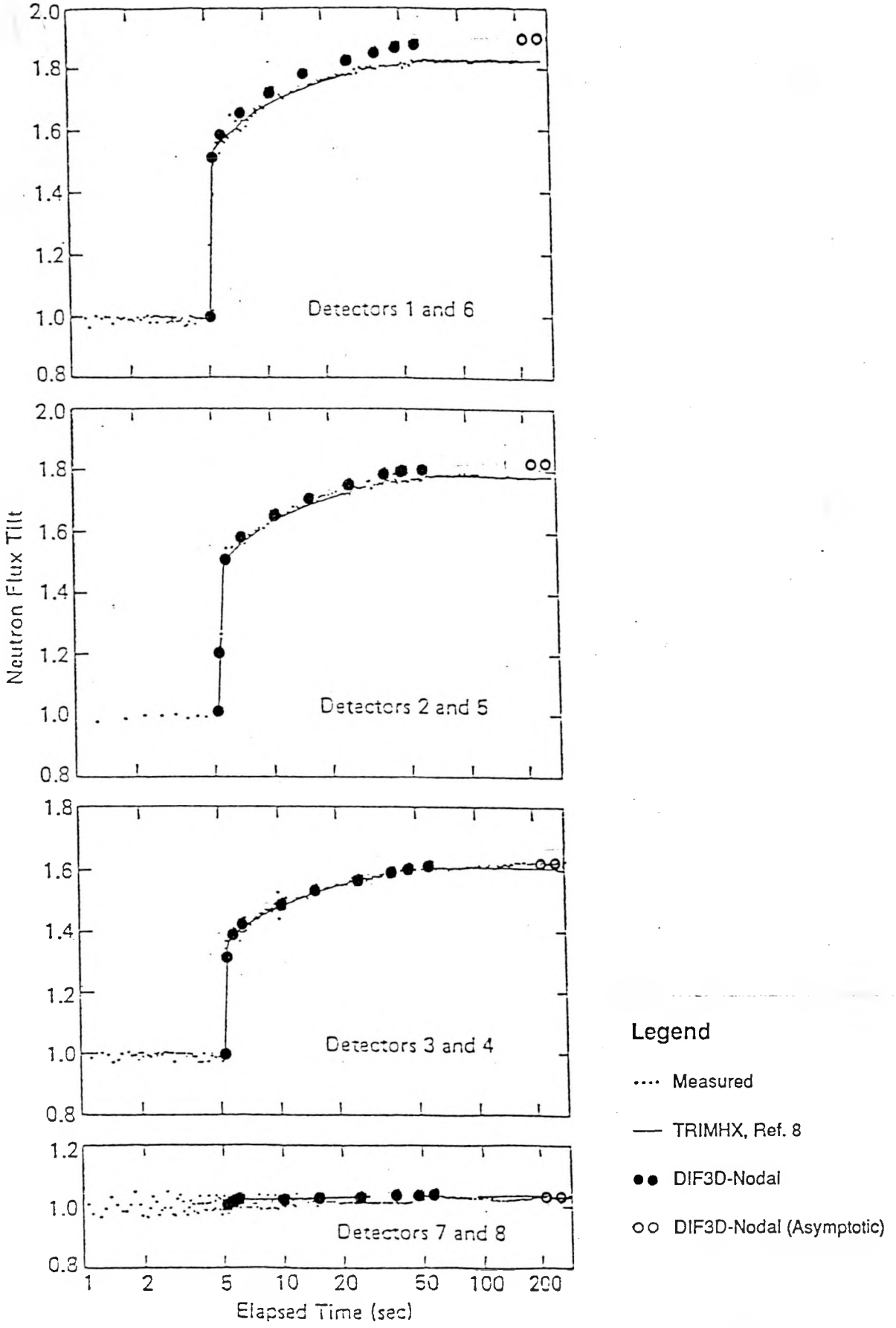

Figure 6. Measured and Calculated Flux Tilts from Experiment 2.